Letter

Increased atom-cavity coupling through cooling-induced atomic reorganization

Chi Shu,[1,2,*] Simone Colombo,[1,*,†] Zeyang Li,[1,*,‡] Albert Adiyatullin,[1,§] Enrique Mendez,[1] Edwin Pedrozo-Peñafiel,[1,‖] and Vladan Vuletić[1,¶]

[1]*Department of Physics, MIT-Harvard Center for Ultracold Atoms and Research Laboratory of Electronics, Massachusetts Institute of Technology, Cambridge, Massachusetts 02139, USA*

[2]*Department of Physics, Harvard University, Cambridge, Massachusetts 02138, USA*

(Received 17 October 2023; accepted 14 August 2024; published 3 September 2024)

The strong coupling of atoms to optical cavities can improve optical lattice clocks as the cavity enables metrologically useful collective atomic entanglement and high-fidelity measurement. To this end, it is necessary to cool the ensemble to suppress motional broadening, and advantageous to maximize and homogenize the atom-cavity coupling. We demonstrate resolved Raman sideband cooling via the cavity as a method that can simultaneously achieve both goals. In 200 ms of Raman sideband cooling, we cool ^{171}Yb atoms to an average vibration number $\langle n_x \rangle = 0.23(7)$ in the tightly binding direction, resulting in 93% optical π-pulse fidelity on the clock transition $^1S_0 \rightarrow {}^3P_0$. During cooling, the atoms self-organize into locations with maximal atom-cavity coupling, which will improve quantum metrology applications.

DOI: 10.1103/PhysRevResearch.6.L032049

Ultracold atomic ensembles in optical cavities constitute a versatile platform for a wide range of applications, from generating nonclassical states of light [1–4], to mediating the atom-atom interaction for quantum metrology [5–12], quantum information science [13–16], and quantum many-body physics [17–29]. In particular, the strong cavity-atom interaction has been harnessed for atomic-clock operation [30–33], as the cavity offers substantially increased photon collection efficiency for atomic-state measurement [34], provides a high-power trapping lattice, and enables the engineering of atomic collective entangled states, such as spin squeezed states [35], to enhance the precision of clock phase estimation below the standard quantum limit [5–12].

For most of these applications, ideally, the coupling between the cavity field and each atom should be independent of each atom's location and motion. This translates to two technical challenges in such systems: how to overcome the inhomogeneous coupling of the atoms to the light mode in standing-wave cavities due to the incommensurability between the trapping and interaction standing waves, and how to reduce the temperature and thus the thermal noise and motional dephasing. The coupling can be made homogeneous by selectively removing weakly coupled atoms [36], at the expense of reduced atom number. Alternatively, one can use wavelength-commensurate trapping and interaction optical lattices [37]. However, the latter is not possible in optical lattice clocks that require a particular (magical) trapping wavelength [38].

Concerning thermal noise, direct laser cooling to Bose-Einstein condensation on a narrow transition [39,40] and by Raman cooling in alkali metal atoms [41–43] have demonstrated the ability to cool to quantum degeneracy with relatively simple experimental setups. However, this has not yet been demonstrated on a ytterbium system, because the laser cooling relies on the thermalization process through elastic collisions that occur during the cooling, whereas for ^{171}Yb, the relevant collision cross section is smaller by three orders of magnitude than both alkali atoms and other optical-clock candidates such as ^{87}Sr.

In this Letter, we report a high-finesse cavity ($\mathcal{F} = 12\,000$) assisted two-photon Raman sideband cooling method for ^{171}Yb atoms that simultaneously cools to the quantum ground state in the tightly confined directions in a magic wavelength trap (lattice spacing $\lambda/2 \approx 380$ nm), and reorganizes the atoms along the cavity axis to achieve a stronger and uniform coupling to the cavity. The cooling relies on one cavity-enhanced laser and a transverse laser beam, both at 556 nm near the $^1S_0 \rightarrow {}^3P_1$ transition. This setup reduces the complexity of the optical setup, compared with the previous approaches, which used 567 and 1388-nm lasers to drive the $^1S_0 \rightarrow {}^3P_0 \rightarrow {}^3D_1$ cooling transitions [44,45]. The attained low mean vibrational quantum number $\langle n_x \rangle = 0.23(7)$ enables high-fidelity Rabi oscillations on the $^1S_0 \rightarrow$

*These authors contributed equally to this work.
†Present address: Department of Physics, University of Connecticut, Storrs, Connecticut 06269, USA.
‡Present address: Department of Applied Physics, Stanford University, Stanford, California 94305, USA.
§Present address: Quandela, 7 Rue Leonard de Vinci, 91300 Massy, France.
‖Present address: Department of Physics, University of Florida, Gainesville, Florida 32611, USA.
¶Contact author: vuletic@mit.edu

$^3P_0$ optical-clock transition, which in combination with the cavity enables entanglement-induced metrological gain [30]. Due to the very small elastic collision cross section of ^{171}Yb, the temperatures along the tightly confined direction [$T_x = 1.8(2)$ μK] and the weakly confined direction [$T_y = 8(3)$ μK] remain decoupled even at atomic densities of $n \sim 10^{11}$ cm^{-3}. One feature of the cooling is that the atoms also reorganize along the cavity towards the trapping positions with larger coupling to the cavity, thereby increasing the effective single-atom cooperativity η to within 5% of its maximum value. At the same time, the phase space density (maximum occupation per quantum state) increases to PSD = 0.013(3), bringing the system close to quantum degeneracy.

Atoms are first loaded into a bicolor mirror magneto-optical trap (MOT) [46,47] located inside the optical cavity. By changing the bias magnetic fields, we adjust the MOT to overlap well with the vertical (z) cavity mode and a one-dimensional standing-wave optical lattice in the x direction with a waist of 27 μm. The x-direction lattice operates at the magic wavelength (759 nm) for the $|\,^1S_0\rangle \rightarrow |\,^3P_0\rangle$ clock transition, and has a trap depth $U_x/h = 460$ kHz. The x lattice is necessary to localize the atoms and remove the Doppler broadening for the $|\,^1S_0\rangle \rightarrow |\,^3P_0\rangle$ clock probe light propagating along the same direction.

We then turn off the MOT beams and send a second magic-wavelength trapping beam into the cavity to generate an optical lattice along the z direction with a waist of 130 μm and trap depth $U_z/h = 2$ MHz at the atoms' position. The corresponding vibration frequencies of atoms in the two-dimensional (2D) optical lattice are $\{\omega_x/(2\pi), \omega_y/(2\pi), \omega_z/(2\pi)\} = \{60, 1, 130\}$ kHz. To remove any atoms outside the 2D trap overlap region, the optical lattice along x is adiabatically ramped down, held off for 50 ms, and then slowly ramped back up in 15 ms, followed by a ramping down and back up of the cavity trap light in 32 ms. This procedure results in a cloud of ∼500 ^{171}Yb atoms with root-mean-square (rms) sizes of 16 and 4.8 μm along the z and x, y directions, respectively. At this point, the peak local density and peak phase space density in the two-dimensional lattice are $n_0 = 3 \times 10^{11}$ cm^{-3} and PSD $= 2 \times 10^{-4}$, respectively.

Both the Raman coupling and the optical pumping necessary for the Raman sideband cooling [41,48,49] are accomplished with a laser near the $^1S_0 \rightarrow {}^3P_1$ transition. The optical pumping is performed with a σ^+-polarized beam along the cavity that is resonant with the $|\,^1S_0, m_F = -\frac{1}{2}\rangle \rightarrow |^3P_1, m_F = +\frac{1}{2}\rangle$ transition, while the Raman coupling uses two beams detuned from the $|\,^1S_0, -\frac{1}{2}\rangle \rightarrow |^3P_1, +\frac{1}{2}\rangle$ transition by $\Delta/(2\pi) = -10$ MHz, one σ^+-polarized beam along the cavity, and a π-polarized beam in the xy plane (see Fig. 1). With a B field of 13.5 G along the z axis, the relative detuning of those two beams is chosen to match the $|\,^1S_0, m_F = \frac{1}{2}, n_x\rangle \rightarrow |\,^1S_0, m_F = -\frac{1}{2}, n_x - 1\rangle$ transition between the two ground states that reduces the vibrational quantum number n_x by one, and hence the motional energy by $E/h = 60$ kHz. The optical pumping back to the $|m_F = -\frac{1}{2}\rangle$ state heats the atom on average by $2E_{\rm rec}/h = 7.4$ kHz, where $E_{\rm rec}$ is the recoil energy for the $^1S_0 \rightarrow {}^3P_1$ transition. After cooling for a variable time (1–1000 ms), we extinguish the Raman beams 5 ms before the optical-pumping light in order to initialize the atoms in the $|\,^1S_0, m_F = \frac{1}{2}\rangle$ level. After the cooling process, the optical lattice along the z direction is ramped down to 30% of its initial power to reduce the photon scattering by the trap light.

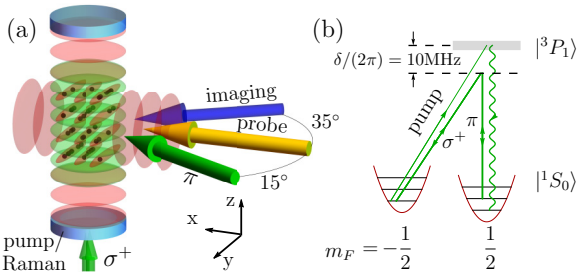

FIG. 1. Raman sideband cooling in an optical cavity. (a) A cavity along the vertical z direction supports both a trapping optical lattice at 759 nm and light near the $|^1S_0, m_F = \frac{1}{2}\rangle \rightarrow |^3P_1, m_F = \frac{3}{2}\rangle$ transition at 556 nm for optical pumping, serving as one leg of the Raman transition. An additional π-polarized Raman beam is applied in the xy plane at an angle of 15° relative to the x axis. The laser beam driving the $|^1S_0\rangle \rightarrow |^3P_0\rangle$ optical-clock transition propagates along x; so does an additional transverse 759-nm optical lattice. Time-of-flight imaging on the $^1S_0 \rightarrow {}^1P_1$ transition at 399 nm is performed at 35° against the x direction in the xy plane. (b) With $B_z = 13.5$ G, Zeeman splittings in $^3P_1$ and $^1S_0$ are 20 MHz and 10 kHz, respectively. Raman beams are red detuned by 10 MHz to the $|^1S_0, m_F = \frac{1}{2}\rangle \rightarrow |^3P_1, m_F = \frac{1}{2}\rangle$ transitions with the resonant two-photon condition between the two ground states.

The atomic temperature is determined by spectroscopy on the clock transition $^1S_0 \rightarrow {}^3P_0$ using a π-polarized laser beam traveling along the x direction. This laser is stabilized to an ultralow-expansion cavity and measures the population of vibrational states via sideband spectroscopy [50], as shown in Fig. 2. The broad Gaussian background underlying the discrete sideband spectrum is attributed to the Doppler profile of floating atoms that are not confined in a single site of the

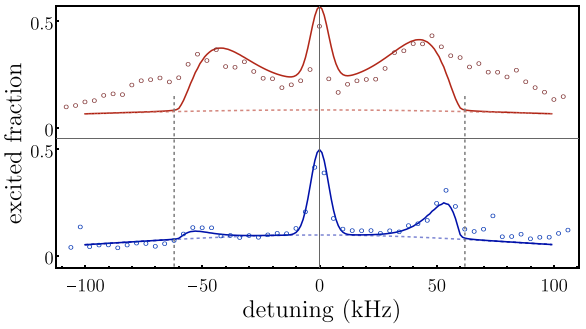

FIG. 2. Clock state excitation spectroscopy ($|\,^1S_0\rangle \rightarrow |^3P_0\rangle$) in the 2D optical lattice (a) before and (b) after 200 ms of cooling. Clock pulse lengths of (a) 5 ms and (b) 20 ms are applied. At high temperature, there is a large Doppler broadened background of atoms that are only trapped by the intracavity light. At low temperatures, the vibrational sidebands in the x lattice are prominent, and the red sideband is suppressed. Assuming a thermal distribution, the fitted temperatures of the cloud are $T_{x,i} = 20(2)$ μK before cooling and $T_{x,f} = 1.8(5)$ μK after cooling, with mean vibrational occupation numbers $\langle n_{x,i}\rangle = 6.1(7)$ and $\langle n_{x,f}\rangle = 0.23(4)$, respectively.

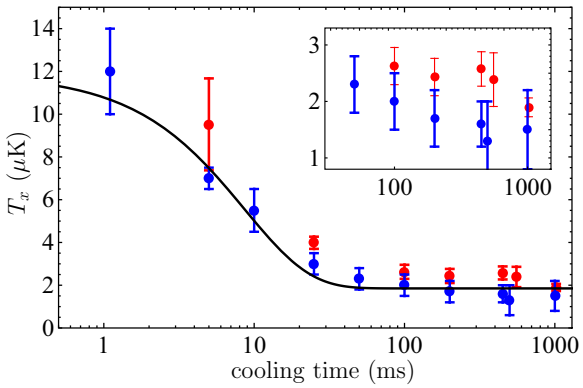

FIG. 3. Temperature as a function of cooling time. Blue data represent the temperature obtained by sideband analysis (see Fig. 2) while red data are obtained by fitting the Rabi flopping to the theory from Ref. [50]. The solid line is an exponential decay fit of the blue data, with a cooling time constant of 9(1) ms, and a final temperature of 1.8(5) μK. The inset shows the temperature trend at late times.

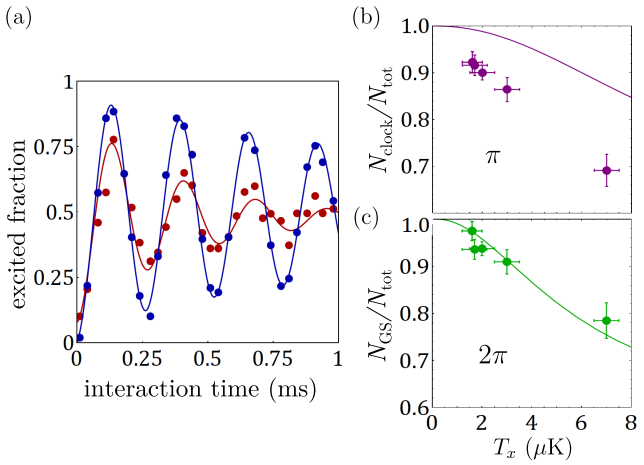

FIG. 4. (a) Rabi flopping on the clock transition $|{}^1S_0\rangle \rightarrow |{}^3P_0\rangle$ for different temperatures ($T = 1.8$ μK, blue data points, and $T = 10$ μK, red data points). The deviation from the theory [50] for the π pulse [purple points in (b)] is due to the fraction of atoms that are not confined in the 2D lattice. This fraction increases when the temperature is higher. The 2π pulse (c) is insensitive to those unconfined atoms, and measures the contrast of those atoms that participate in the Rabi flopping.

lattice along x, but are confined in the intracavity trap with a much larger trap depth. Before the cooling, the blue and red sidebands have a similar size, which indicates a mean vibrational quantum number $n_x \gg 1$, while the Doppler background in the spectrum implies a large portion of atoms that are not confined in the x lattice. By fitting the spectroscopy data to the model [50], we obtain an initial cloud temperature of $T_{x,i} = 20(2)$ μK. After 200 ms of Raman sideband cooling, a large sideband imbalance is observed, implying that the atoms are cooled to near the vibrational ground state with $\langle n_x \rangle = 0.23(7)$ which corresponds to a final temperature of $T_{x,f} = 1.8(5)$ μK. The reduced residual Doppler background indicates that atoms originally not confined by the x lattice are cooled to the vibrational ground state as well. Figure 3 shows a fast initial cooling within the first 10 ms, followed by a slower temperature decrease as the atoms are cooled into the ground state.

After the cooling, the optical Rabi oscillation experiences a much smaller dephasing than before the cooling, resulting in strongly improved coherent transfer to the excited clock state $|{}^3P_0\rangle$ [Fig. 4(a)]. After 200 ms of cooling, the transfer fidelity reaches 0.93(3). The remaining infidelity can be explained by the residual population of vibrational excited states, which experience different Rabi frequencies Ω_m on the $|{}^1S_0, n_z = m\rangle \rightarrow |{}^3P_0, n_z = m\rangle$ vibrational transition, given by $\Omega_m = \Omega_0 e^{-\eta_x^2/2} L_n(\eta_x^2)$. Here, Ω_0 is the Rabi frequency for the vibrational ground state, $\eta_x = 0.24(1)$ is the Lamb-Dicke parameter for our lattice depth, and L_n is the Laguerre polynomial. When we compare the π-pulse and 2π-pulse fidelities [Figs. 4(a) and 4(b)] to each other and to a model [50], we observe deviations. We believe that those deviations arise from residual atoms with high kinetic energy, which are trapped by the trapping potential envelope but do not localize inside the lattice tube. We see that the π-pulse fidelity is lower and deviates more from the model, whereas the 2π pulse is insensitive to those atoms.

From Fig. 3, we notice that for cooling times $t > 30$ ms, the temperature barely changes, and this is also true for the π-pulse fidelity after the corresponding cooling time. However, when we measure the effective atom number via the vacuum Rabi splitting of the cavity mode [11], we find that the collective cooperativity $N\eta$ evolves with a quite different timescale from the temperature [see Fig. 5(a)]. The collective cooperativity $N\eta$ increases at first, and later drops below its original value. Since the atom number N can only decrease during the interaction with the cooling light, we conclude that the cavity coupling per atom [effective single-atom cooperativity η—see Supplemental Material (SM) [51]] is increasing during the cooling. This implies that the atoms must be reorganizing themselves along the cavity axis towards lattice trapping sites that have a stronger coupling to the cavity probe light. This reorganization is on the 2-μm scale, given by the beat note between the trapping light and the probe light.

To extract the single-atom cooperativity, we then measure the quantum projection noise of a coherent spin state after cooling for different atom numbers (see SM [51]). The spin quantum projection noise scales with the square root of the atom number N, while the total coupling strength $N\eta$ scales linearly with N. Therefore, comparing the spin noise variance with $N\eta$, the effective single-atom cooperativity η can be deduced [52]. Figure 5(b) shows that η increases during the cooling until it saturates at 200 ms. Prior to the cooling process, the atoms are homogeneously distributed along the magic-wavelength lattice that has a different wavelength from the probing lattice near the $|{}^1S_0\rangle \rightarrow |{}^3P_1\rangle$ transition. The increase in single-atom cooperativity implies a redistribution of the atoms towards trapping sites with increased coupling to the probe light. [The radial cooling can also increase the single-atom cooperativity, but at most by 13% (see SM [51]), while we observe a larger increase of 30%.] If the increase in effective single-atom cooperativity beyond the transverse compression were due to the removal of weakly coupled atoms as demonstrated in Ref. [36], we would obtain the

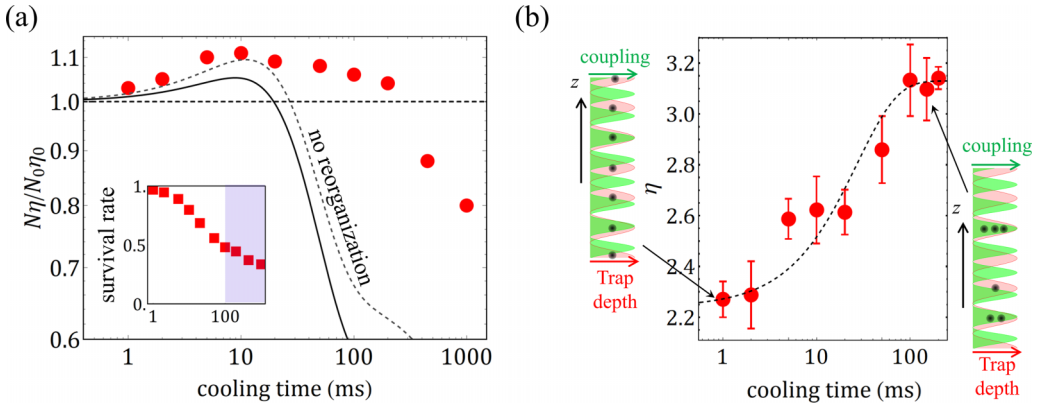

FIG. 5. Cavity coupling during the cooling process. (a) Collective cooperativity $N\eta$, normalized to the initial value, vs cooling time. The two lines are obtained with a model based on the absence of atomic reorganization during the cooling process, i.e., weakly trapped atoms are lost. The solid line considers a transverse cooling-induced compression occurring along the weakly trapped direction, while the dashed line represents the case of an isotropic compression. The inset shows the inferred survival rate $N_{\rm tot}(t)/N_{\rm tot}(0)$ as a function of the cooling time t. Details and validation of the model are presented in the Supplemental Material [51]. (b) Effective cooperativity as a function of the cooling time. The dashed line is a fit of an exponential decay with an offset and serves as a guide to the eye. Insets: The schematic of atomic distribution among the incommensurate trapping and coupling lattices. Initially, atoms are evenly distributed in the trapping lattice, and after long-time cooling, the atoms are concentrated in lattice sites with strong coupling to the cavity probe light.

black solid line in Fig. 5(a), which disagrees with the data. The much higher remaining $N\eta$ in spite of atom loss requires a reorganization of atomic distribution along the cavity axis during cooling towards trapping sites with large coupling to the cavity probe light.

We attribute the reorganization of the atoms along the cavity mode to the spatially dependent optical pumping and cooling that is performed with light in the same longitudinal and transverse cavity mode as the probe light. This means that atoms that are trapped in magic-wavelength lattice sites that are strongly coupled to the optical-pumping lattice experience strong cooling, while atoms that are trapped in sites that are weakly or not coupled to the optical-pumping light are not cooled but experience photon recoil heating due to light scattering from the π-polarized Raman beam illuminating them from the side. Atoms that were originally loaded into such sites are then likely to be heated out, and can migrate to sites with good optical pumping and cooling, where they will be cooled deeply into the lattice. The latter sites are also strongly coupled to the probe light in the same mode, resulting in larger single-atom cooperativity. The observed timescale for the reorganization of the atoms along the vertical cavity lattice of ∼50 ms (see Fig. 5) is much longer than the ∼10 ms timescale for local cooling.

After 200 ms of cooling, the rms sizes of the atomic ensemble are $z_0 = 12$ μm and $x_0 = 3.2$ μm, resulting in a peak occupation of $N_{\rm tube} = 1.1$ atoms per tube. Even though the loaded atom number or atom survival during cooling were not optimized, the peak PSD of $1.3(3) \times 10^{-2}$ is already within a factor of 70 of quantum degeneracy (albeit currently at only one atom per tube). We believe that by using methods developed for Sr [39,40] and the alkalis [41–43], such as spectral shielding [39] and spatial compression and recooling, it should be possible to reach quantum degeneracy by Raman sideband cooling in ^{171}Yb. This would generalize the optical cooling to quantum degeneracy method into Fermionic atoms.

In conclusion, we have demonstrated Raman sideband cooling of nearly noncolliding atoms to near the motional ground state in two directions. This enables high-fidelity Rabi flopping on the optical-clock transition that is crucial for clock operation [50,53,54] and precision beyond the standard quantum limit [30,33]. In the future, a similar approach with improved optical access can likely be used to directly laser cool the fermionic gas to quantum degeneracy at small atom loss and in a cooling time substantially shorter than standard approaches with evaporative cooling.

This work was supported by NSF (Grant No. PHY-1806765), DARPA (Grant No. D18AC00037), ONR (Grant No. N00014-20-1-2428), the NSF Center for Ultracold Atoms (CUA) (Grant No. PHY-1734011).

[1] C. Sayrin, I. Dotsenko, X. Zhou, B. Peaudecerf, T. Rybarczyk, S. Gleyzes, P. Rouchon, M. Mirrahimi, H. Amini, M. Brune, J.-M. Raimond, and S. Haroche, Real-time quantum feedback prepares and stabilizes photon number states, Nature (London) **477**, 73 (2011).

[2] B. Vlastakis, G. Kirchmair, Z. Leghtas, S. E. Nigg, L. Frunzio, S. M. Girvin, M. Mirrahimi, M. H. Devoret, and R. J. Schoelkopf, Deterministically encoding quantum information using 100-photon Schrödinger cat states, Science **342**, 607 (2013).

[3] B. Hacker, S. Welte, G. Rempe, and S. Ritter, A photon-photon quantum gate based on a single atom in an optical resonator, Nature (London) **536**, 193 (2016).

[4] J. Ramette, J. Sinclair, Z. Vendeiro, A. Rudelis, M. Cetina, and V. Vuletić, Any-to-any connected cavity-mediated architecture for quantum computing with trapped ions or Rydberg arrays, PRX Quantum **3**, 010344 (2022).

[5] I. D. Leroux, M. H. Schleier-Smith, and V. Vuletić, Implementation of cavity squeezing of a collective atomic spin, Phys. Rev. Lett. **104**, 073602 (2010).

[6] M. H. Schleier-Smith, I. D. Leroux, and V. Vuletić, States of an ensemble of two-level atoms with reduced quantum uncertainty, Phys. Rev. Lett. **104**, 073604 (2010).

[7] J. G. Bohnet, K. C. Cox, M. A. Norcia, J. M. Weiner, Z. Chen, and J. K. Thompson, Reduced spin measurement back-action for a phase sensitivity ten times beyond the standard quantum limit, Nat. Photon. **8**, 731 (2014).

[8] K. C. Cox, G. P. Greve, J. M. Weiner, and J. K. Thompson, Deterministic squeezed states with collective measurements and feedback, Phys. Rev. Lett. **116**, 093602 (2016).

[9] O. Hosten, N. J. Engelsen, R. Krishnakumar, and M. A. Kasevich, Measurement noise 100 times lower than the quantum-projection limit using entangled atoms, Nature (London) **529**, 505 (2016).

[10] O. Hosten, R. Krishnakumar, N. J. Engelsen, and M. A. Kasevich, Quantum phase magnification, Science **352**, 1552 (2016).

[11] B. Braverman, A. Kawasaki, E. Pedrozo-Peñafiel, S. Colombo, C. Shu, Z. Li, E. Mendez, M. Yamoah, L. Salvi, D. Akamatsu, Y. Xiao, and V. Vuletić, Near-unitary spin squeezing in ^{171}Yb, Phys. Rev. Lett. **122**, 223203 (2019).

[12] Y. Zhao, R. Zhang, W. Chen, X.-B. Wang, and J. Hu, Creation of Greenberger-Horne-Zeilinger states with thousands of atoms by entanglement amplification, npj Quantum Inf. **7**, 24 (2021).

[13] T. Pellizzari, S. A. Gardiner, J. I. Cirac, and P. Zoller, Decoherence, continuous observation, and quantum computing: A cavity QED model, Phys. Rev. Lett. **75**, 3788 (1995).

[14] L.-M. Duan and H. J. Kimble, Scalable photonic quantum computation through cavity-assisted interactions, Phys. Rev. Lett. **92**, 127902 (2004).

[15] H. J. Kimble, The quantum internet, Nature (London) **453**, 1023 (2008).

[16] C. Weedbrook, S. Pirandola, R. García-Patrón, N. J. Cerf, T. C. Ralph, J. H. Shapiro, and S. Lloyd, Gaussian quantum information, Rev. Mod. Phys. **84**, 621 (2012).

[17] H. Ritsch, P. Domokos, F. Brennecke, and T. Esslinger, Cold atoms in cavity-generated dynamical optical potentials, Rev. Mod. Phys. **85**, 553 (2013).

[18] C.-L. Hung, A. González-Tudela, J. I. Cirac, and H. Kimble, Quantum spin dynamics with pairwise-tunable, long-range interactions, Proc. Natl. Acad. Sci. USA **113**, E4946 (2016).

[19] J. Léonard, A. Morales, P. Zupancic, T. Esslinger, and T. Donner, Supersolid formation in a quantum gas breaking a continuous translational symmetry, Nature (London) **543**, 87 (2017).

[20] J. Léonard, A. Morales, P. Zupancic, T. Donner, and T. Esslinger, Monitoring and manipulating Higgs and Goldstone modes in a supersolid quantum gas, Science **358**, 1415 (2017).

[21] V. D. Vaidya, Y. Guo, R. M. Kroeze, K. E. Ballantine, A. J. Kollár, J. Keeling, and B. L. Lev, Tunable-range, photon-mediated atomic interactions in multimode cavity QED, Phys. Rev. X **8**, 011002 (2018).

[22] Y. Guo, V. D. Vaidya, R. M. Kroeze, R. A. Lunney, B. L. Lev, and J. Keeling, Emergent and broken symmetries of atomic self-organization arising from Gouy phase shifts in multimode cavity QED, Phys. Rev. A **99**, 053818 (2019).

[23] Y. Guo, R. M. Kroeze, V. D. Vaidya, J. Keeling, and B. L. Lev, Sign-changing photon-mediated atom interactions in multimode cavity quantum electrodynamics, Phys. Rev. Lett. **122**, 193601 (2019).

[24] A. Morales, D. Dreon, X. Li, A. Baumgärtner, P. Zupancic, T. Donner, and T. Esslinger, Two-mode Dicke model from nondegenerate polarization modes, Phys. Rev. A **100**, 013816 (2019).

[25] E. J. Davis, G. Bentsen, L. Homeier, T. Li, and M. H. Schleier-Smith, Photon-mediated spin-exchange dynamics of spin-1 atoms, Phys. Rev. Lett. **122**, 010405 (2019).

[26] G. Bentsen, T. Hashizume, A. S. Buyskikh, E. J. Davis, A. J. Daley, S. S. Gubser, and M. Schleier-Smith, Treelike interactions and fast scrambling with cold atoms, Phys. Rev. Lett. **123**, 130601 (2019).

[27] G. Bentsen, I.-D. Potirniche, V. B. Bulchandani, T. Scaffidi, X. Cao, X.-L. Qi, M. Schleier-Smith, and E. Altman, Integrable and chaotic dynamics of spins coupled to an optical cavity, Phys. Rev. X **9**, 041011 (2019).

[28] A. J. Park, J. Trautmann, N. Šantić, V. Klüsener, A. Heinz, I. Bloch, and S. Blatt, Cavity-enhanced optical lattices for scaling neutral atom quantum technologies to higher qubit numbers, PRX Quantum **3**, 030314 (2022).

[29] S. Langenfeld, P. Thomas, O. Morin, and G. Rempe, Quantum repeater node demonstrating unconditionally secure key distribution, Phys. Rev. Lett. **126**, 230506 (2021).

[30] E. Pedrozo-Peñafiel, S. Colombo, C. Shu, A. F. Adiyatullin, Z. Li, E. Mendez, B. Braverman, A. Kawasaki, D. Akamatsu, Y. Xiao *et al.*, Entanglement on an optical atomic-clock transition, Nature (London) **588**, 414 (2020).

[31] W. Bowden, A. Vianello, I. R. Hill, M. Schioppo, and R. Hobson, Improving the Q factor of an optical atomic clock using quantum nondemolition measurement, Phys. Rev. X **10**, 041052 (2020).

[32] M.-Z. Huang, J. A. de la Paz, T. Mazzoni, K. Ott, P. Rosenbusch, A. Sinatra, C. L. Garrido Alzar, and J. Reichel, Observing spin-squeezed states under spin-exchange collisions for a second, PRX Quantum **4**, 020322 (2023).

[33] J. M. Robinson, M. Miklos, Y. M. Tso, C. J. Kennedy, T. Bothwell, D. Kedar, J. K. Thompson, and J. Ye, Direct comparison of two spin-squeezed optical clock ensembles at the 10^{-17} level, Nat. Phys. **20**, 208 (2024).

[34] H. Tanji-Suzuki, I. D. Leroux, M. H. Schleier-Smith, M. Cetina, A. T. Grier, J. Simon, and V. Vuletić, Interaction between atomic ensembles and optical resonators: Classical description, in *Advances in Atomic, Molecular, and Optical Physics*, edited by P. B. E. Arimondo and C. Lin (Academic Press, London, 2011), Vol. 60, Chap. 4, pp. 201–237.

[35] M. Kitagawa and M. Ueda, Squeezed spin states, Phys. Rev. A **47**, 5138 (1993).

[36] B. Wu, G. P. Greve, C. Luo, and J. K. Thompson, Site-dependent selection of atoms for homogeneous atom-cavity coupling, arXiv:2104.01201.

[37] J. Lee, G. Vrijsen, I. Teper, O. Hosten, and M. A. Kasevich, Many-atom–cavity QED system with homogeneous atom–cavity coupling, Opt. Lett. **39**, 4005 (2014).

[38] H. Katori, M. Takamoto, V. G. Pal'chikov, and V. D. Ovsiannikov, Ultrastable optical clock with neutral atoms in an engineered light shift trap, Phys. Rev. Lett. **91**, 173005 (2003).

[39] S. Stellmer, B. Pasquiou, R. Grimm, and F. Schreck, Laser cooling to quantum degeneracy, Phys. Rev. Lett. **110**, 263003 (2013).

[40] C.-C. Chen, R. González Escudero, J. Minář, B. Pasquiou, S. Bennetts, and F. Schreck, Continuous Bose–Einstein condensation, Nature (London) **606**, 683 (2022).

[41] J. Hu, A. Urvoy, Z. Vendeiro, V. Crépel, W. Chen, and V. Vuletić, Creation of a Bose-condensed gas of ^{87}Rb by laser cooling, Science **358**, 1078 (2017).

[42] P. Solano, Y. Duan, Y.-T. Chen, A. Rudelis, C. Chin, and V. Vuletić, Strongly correlated quantum gas prepared by direct laser cooling, Phys. Rev. Lett. **123**, 173401 (2019).

[43] Z. Vendeiro, J. Ramette, A. Rudelis, M. Chong, J. Sinclair, L. Stewart, A. Urvoy, and V. Vuletić, Machine-learning-accelerated Bose-Einstein condensation, Phys. Rev. Res. **4**, 043216 (2022).

[44] N. Nemitz, T. Ohkubo, M. Takamoto, I. Ushijima, M. Das, N. Ohmae, and H. Katori, Frequency ratio of Yb and Sr clocks with 5×10^{-17} uncertainty at 150 seconds averaging time, Nat. Photon. **10**, 258 (2016).

[45] X. Zhang, K. Beloy, Y. S. Hassan, W. F. McGrew, C.-C. Chen, J. L. Siegel, T. Grogan, and A. D. Ludlow, Subrecoil clock-transition laser cooling enabling shallow optical lattice clocks, Phys. Rev. Lett. **129**, 113202 (2022).

[46] A. Kawasaki, B. Braverman, E. Pedrozo-Peñafiel, C. Shu, S. Colombo, Z. Li, O. Özel, W. Chen, L. Salvi, A. Heinz, D. Levonian, D. Akamatsu, Y. Xiao, and V. Vuletić, Geometrically asymmetric optical cavity for strong atom-photon coupling, Phys. Rev. A **99**, 013437 (2019).

[47] A. Kawasaki, B. Braverman, E. Pedrozo-Peñafiel, C. Shu, S. Colombo, Z. Li, and V. Vuletić, Trapping ^{171}Yb atoms into a one-dimensional optical lattice with a small waist, Phys. Rev. A **102**, 013114 (2020).

[48] S. E. Hamann, D. L. Haycock, G. Klose, P. H. Pax, I. H. Deutsch, and P. S. Jessen, Resolved-sideband Raman cooling to the ground state of an optical lattice, Phys. Rev. Lett. **80**, 4149 (1998).

[49] V. Vuletić, C. Chin, A. J. Kerman, and S. Chu, Degenerate Raman sideband cooling of trapped cesium atoms at very high atomic densities, Phys. Rev. Lett. **81**, 5768 (1998).

[50] S. Blatt, J. W. Thomsen, G. K. Campbell, A. D. Ludlow, M. D. Swallows, M. J. Martin, M. M. Boyd, and J. Ye, Rabi spectroscopy and excitation inhomogeneity in a one-dimensional optical lattice clock, Phys. Rev. A **80**, 052703 (2009).

[51] See Supplemental Material at http://link.aps.org/supplemental/10.1103/PhysRevResearch.6.L032049 for additional information, which includes Refs. [25,55–62].

[52] M. H. Schleier-Smith, I. D. Leroux, and V. Vuletić, Squeezing the collective spin of a dilute atomic ensemble by cavity feedback, Phys. Rev. A **81**, 021804(R) (2010).

[53] G. Campbell, M. Boyd, J. Thomsen, M. Martin, S. Blatt, M. Swallows, T. L. Nicholson, T. Fortier, C. W. Oates, S. A. Diddams *et al.*, Probing interactions between ultracold fermions, Science **324**, 360 (2009).

[54] T. Akatsuka, M. Takamoto, and H. Katori, Optical lattice clocks with non-interacting bosons and fermions, Nat. Phys. **4**, 954 (2008).

[55] M. G. Raizen, R. J. Thompson, R. J. Brecha, H. J. Kimble, and H. J. Carmichael, Normal-mode splitting and linewidth averaging for two-state atoms in an optical cavity, Phys. Rev. Lett. **63**, 240 (1989).

[56] P. Münstermann, T. Fischer, P. Maunz, P. W. H. Pinkse, and G. Rempe, Dynamics of single-atom motion observed in a high-finesse cavity, Phys. Rev. Lett. **82**, 3791 (1999).

[57] B. Braverman, Cavity quantum electrodynamics with ensembles of ytterbium-171, Ph.D. thesis, Massachusetts Institute of Technology, 2018.

[58] H. K. Cummins, G. Llewellyn, and J. A. Jones, Tackling systematic errors in quantum logic gates with composite rotations, Phys. Rev. A **67**, 042308 (2003).

[59] M. Bando, T. Ichikawa, Y. Kondo, and M. Nakahara, Concatenated composite pulses compensating simultaneous systematic errors, J. Phys. Soc. Jpn. **82**, 014004 (2013).

[60] B. Braverman, A. Kawasaki, and V. Vuletić, Impact of non-unitary spin squeezing on atomic clock performance, New J. Phys. **20**, 103019 (2018).

[61] A. Kawasaki, Towards spin squeezed ^{171}Yb atomic clock beyond the standard quantum limit, Ph.D. thesis, Massachusetts Institute of Technology, 2017.

[62] J. Hu, W. Chen, Z. Vendeiro, H. Zhang, and V. Vuletić, Entangled collective-spin states of atomic ensembles under nonuniform atom-light interaction, Phys. Rev. A **92**, 063816 (2015).